DOE/SC-ARM/P-08-006

Atmospheric Properties from the 2006 Niamey Deployment and Climate Simulation with a Geodesic Grid Coupled Climate Model

Second Quarter 2008
ARM and Climate Change Prediction Program Report

M. Jensen/Brookhaven National Laboratory
K. Johnson/Brookhaven National Laboratory
J. Mather/Pacific Northwest National Laboratory
D. Randall/Colorado State University

March 2008

Work supported by the U.S. Department of Energy,
Office of Science, Office of Biological and Environmental Research

DISCLAIMER

Contents

Figures

1. Introduction

In 2008, the Atmospheric Radiation Measurement (ARM) Program and the Climate Change Prediction Program (CCPP) have been asked to produce joint science metrics. For CCPP, the metrics will deal with a decade-long control simulation using geodesic grid-coupled climate model. For ARM, the metrics will deal with observations associated with the 2006 deployment of the ARM Mobile Facility (AMF) to Niamey, Niger. Specifically, ARM has been asked to deliver data products for Niamey that describe cloud, aerosol, and dust properties.

2. Cloud Occurrence Frequency from the 2006 ARM Mobile Facility Deployment at Niamey, Niger, Africa

To better understand the energy balance of the earth's atmosphere-ocean system and how this balance will change in the future, a high priority must be placed on quantifying the role of clouds in modulating the energy distribution in the earth's atmosphere and at the surface. Clouds are a critical component of the earth's atmospheric energy balance due to their interaction with solar and terrestrial radiation and redistribution of heat through convective processes and latent heating. The first order quantity needed to understand these impacts is the height of cloud occurrence and how it changes at various timescales.

The ARM Program has defined a specific metric for the second quarter of FY 2008 to, "produce and make available, new continuous time series of cloud frequency, based on results from the ARM Mobile Facility deployment in Niger, Africa." To accomplish this metric, observations from the 95-GHz W-band ARM Cloud Radar (WACR), Micropulse Lidar (MPL), and ceilometer have been combined using the new WACR Active Remote Sensing of Clouds (WACR-ARSCL) value-added product (Kollias et al., 2008) to produce cloud boundaries and time-height profiles of cloud location (among other important radar-observed quantities). From these instantaneous profiles of cloud location, hourly statistics of cloud occurrence frequency as a function of height are compiled and reported in a single annual file.

2.1 Cloud Occurrence Frequency Profiles

The basic algorithm used in the WACR-ARSCL value-added product (VAP) is similar to that employed by the ARSCL VAP, which is based on 35-GHz Millimeter Cloud Radar observations (Clothiaux et al., 2000). It uses a combination of WACR, MPL, and ceilometer observations to produce boundaries and time-height profiles of cloud location, radar moments, and linear depolarization ratio (LDR) fields. The temporal resolution is 5 seconds. The vertical resolution is equal to that of the WACR, 42.856 m.

First, an MPL-based cloud mask is determined based on the comparison of lidar backscatter measurements to returns during known clear-sky periods. Next, a WACR cloud and precipitation mask is derived from signal-to-noise ratio thresholds determined for each time profile. The MPL cloud mask is combined with ceilometer cloud base estimates to produce a best-estimate cloud base for each time. The MPL and WACR cloud masks are merged, then additional filtering of the resulting cloud mask is done in the lower troposphere (below approximately 3.5 km) to remove insect returns. Insects are identified using a combination of WACR LDR and reflectivity measurements. Daily data files include time sequences of cloud boundaries, including ceilometer cloud base, MPL/ceilometer best-estimate cloud base, radar-

derived first cloud top, combined radar-MPL cloud base and top for up to 10 cloud layers for each time, the merged radar-MPL cloud mask, original and masked WACR reflectivity, and masked mean Doppler velocity, spectral width, and LDR.

From these daily files, statistics of cloud occurrence frequency are compiled based on the merged radar-MPL cloud mask. The hourly cloud occurrence frequency for each height bin is calculated as the ratio of the number of positive cloud detections and the number of total observations. A single annual file has been produced that reports this hourly cloud frequency over the Niamey site as a function of time and altitude.

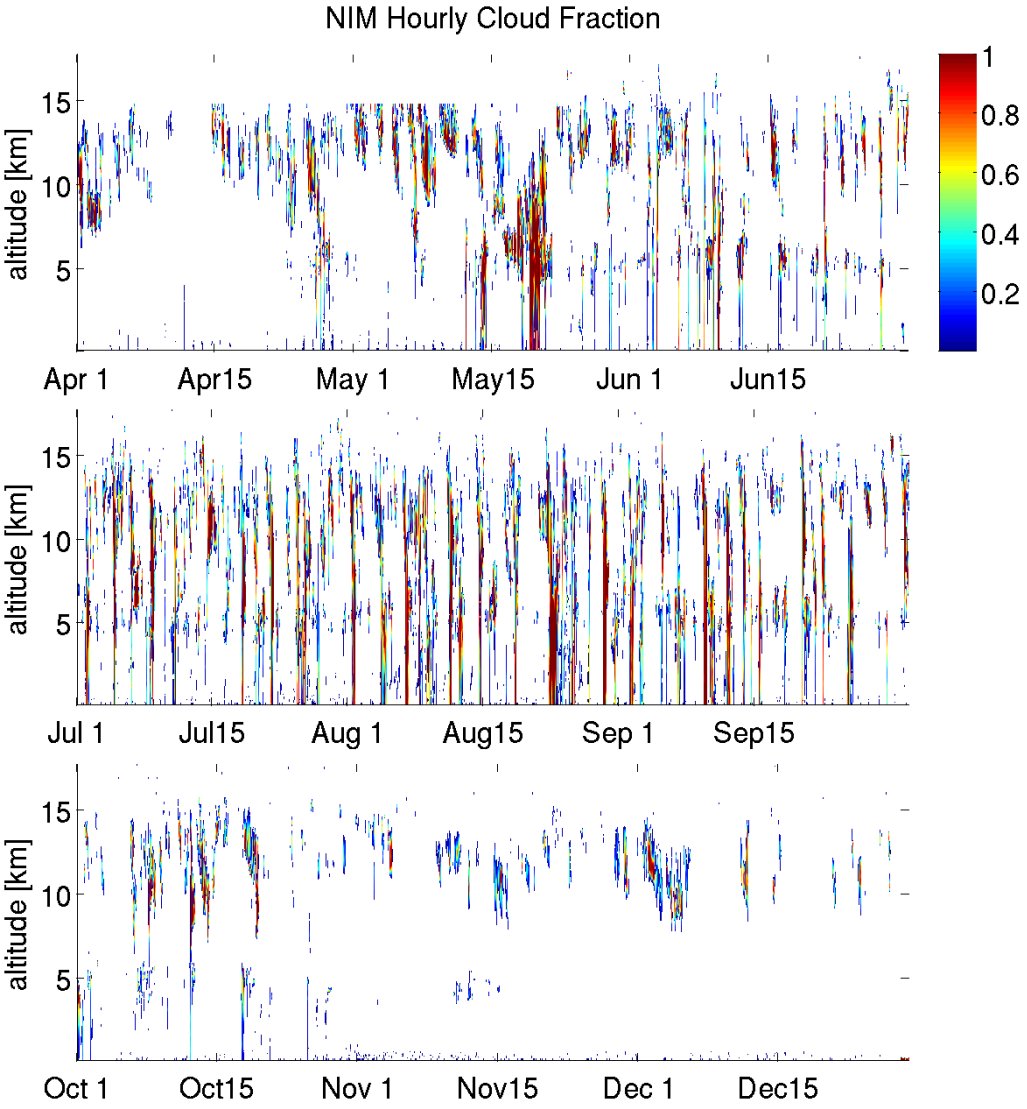

Figure 1: Hourly cloud occurrence frequency at Niamey, Niger, from the AMF WACR-ARSCL value-added product.

The seasonal progression of the West African Monsoon is the greatest source of variability in cloud occurrence at Niamey, Niger. Figure 1 shows the time series of the cloud occurrence frequency for the entire AMF-Niamey deployment. There is a clear distinction between the dry and wet seasons of the West African monsoon. During the dry season (November – April), there is a distinct absence of low-level (< 10 km) clouds. Cirrus clouds advected from outside the region are the only cloud type observed. During the wet season (May – September), there are often clouds present throughout the entire atmospheric column indicating the prevalence of vertically developed convective clouds during this season. Within this season, there is also a notable cycle, on the order of a few days, where convectively active periods are followed by periods where only-high level cirrus and mid-level cumulus congestus clouds are present. Figure 2 illustrates this convective cycle over a period of 10 days in late August. The types of cloud observed during the dry season versus the wet season and within the wet season all have very different impacts on the atmospheric energy balance and water cycle. The observations from the AMF offer the most complete opportunity to quantify the cloud variability within this region and understand its role in climatic feedbacks.

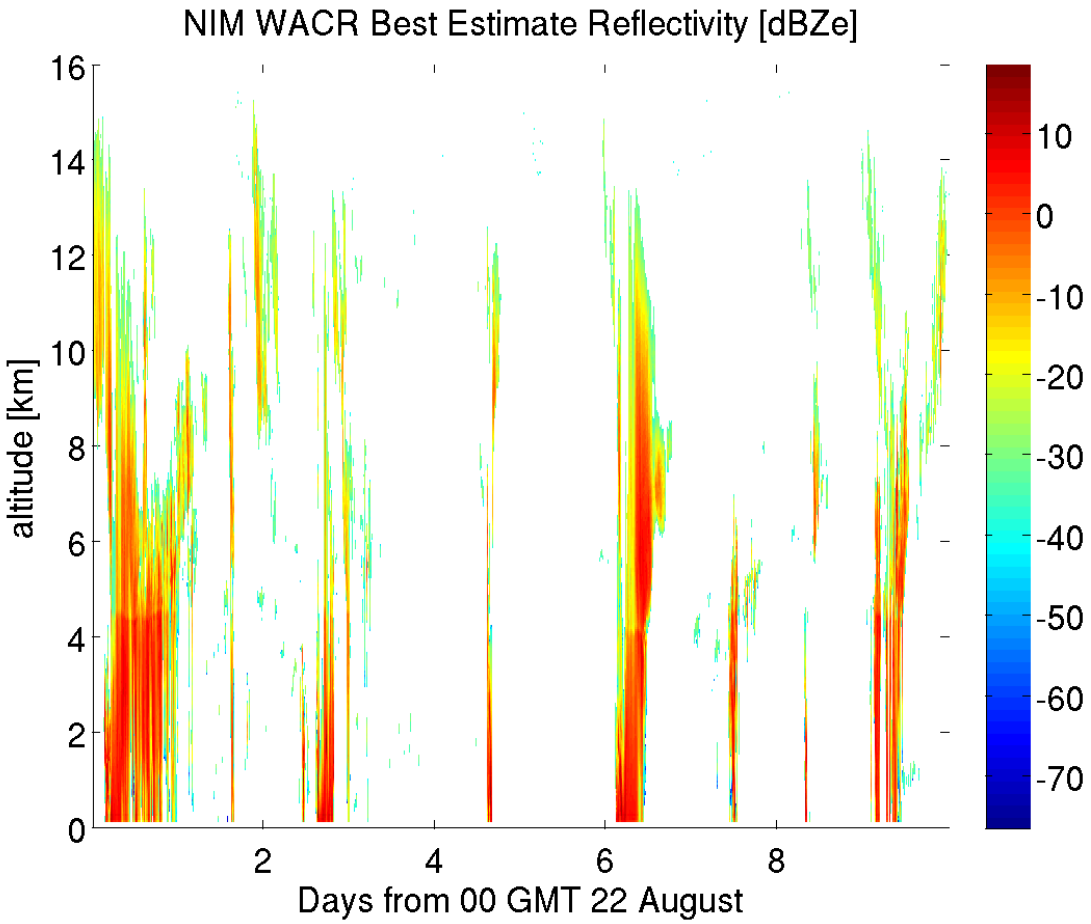

Figure 2: The reflected power from the W-band radar at Niamey for the period August 22 – 31, 2006. This time series illustrates the periodic nature of convection during the Niamey wet season. Hourly cloud frequency is calculated from these detailed radar reflectivity profiles.

2.2 References

Clothiaux, EE, TP Ackerman, GG Mace, KP Moran, RT Marchand, MA Miller, and BE Martner. 2000. "Objective determination of cloud heights and radar reflectivities using a combination of active remote sensors at the ARM CART Sites." *J. Appl. Meteor*. 39, 645-665.

Kollias, P, MA Miller, and KL Johnson. "Cloud and precipitation observations at Niamey during the 2006 ARM Mobile Facility deployment." Submitted to *Geophys. Res. Lett.*

3. A Year-long Control Simulation Using Geodesic Grid Coupled Climate Model at a Resolution ~ 250 km, Including a Comparison With Observations

3.1 Model Description

The Coupled Colorado State Model (CCoSM) is a climate model in which each component is discretized on a geodesic grid (Figure 3) (Heikes and Randall, 1995). A geodesic grid consists of hexagons and pentagons. The grid-cells are relatively uniform across the globe, varying in area by only 5%, and the grid is quasi-isotropic. The distinct climate components in CCoSM are the atmosphere, ocean and sea ice, and their coupling is coordinated by a coupler component which computes the interfacial fluxes and PBL physics. Further description of the model is given in the Appendix.

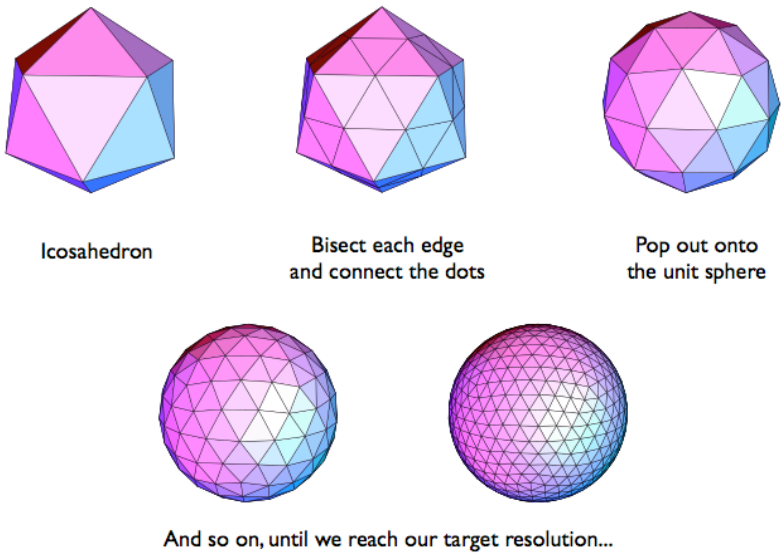

Figure 3: The process used to create a geodesic grid, by starting from an icosahedron.

3.2 Initial Testing in Preparation for a Year-Long Control Simulation Using Geodesic Grid Coupled Climate Model at a Resolution ~ 250 km

3.2.1 Tests of the Atmosphere and Land-Surface Models with Prescribed Sea-Surface Temperatures and Sea Ice

The atmosphere and land-surface models have been subjected to many tests over a period of years. In a particularly important test, we have performed an Atmospheric Model Intercomparison Project (AMIP) simulation (Gates, 1992), in which observed sea-surface temperatures and sea-ice distributions for the years 1979-1988 were prescribed as input. The model results are then analyzed to see if the simulated atmosphere and land surface respond to the year-to-year variations in the sea-surface temperature and sea ice in the same way as observed in the real world. We used a 250-km grid spacing.

An example of the results from our AMIP run is shown in Figure 4, which compares simulated and observed annual-mean total precipitation.

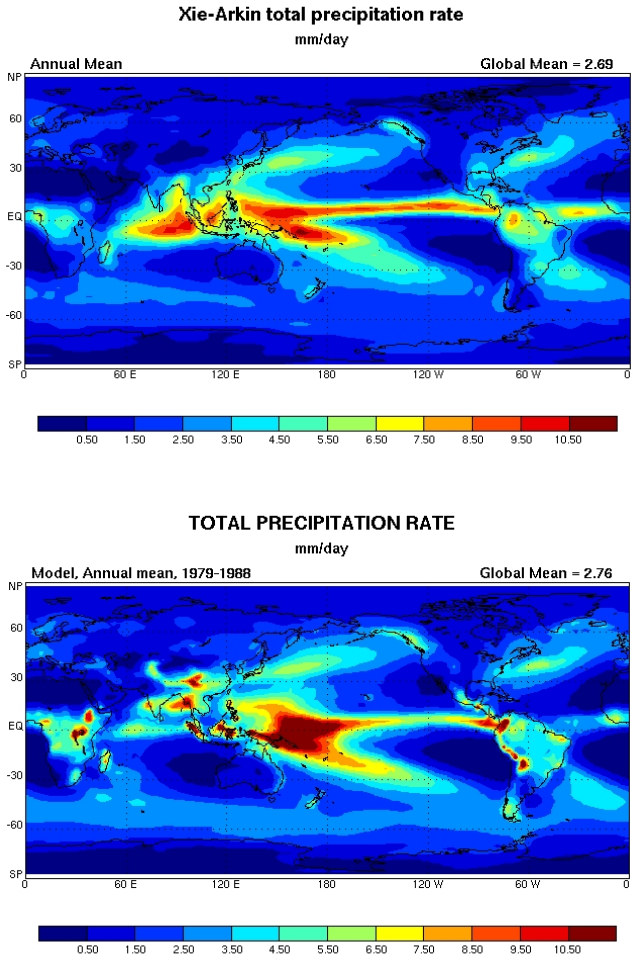

Figure 4: The observed (top panel) and simulated (bottom panel) annual-mean distributions of total precipitation. The simulation is based on an AMIP run, as described in the text.

3.2.2 Tests of the Ocean and Sea-Ice Models with Prescribed Atmospheric Forcing

To test the ocean and sea-ice models, we performed simulations in which the ocean and sea ice are "forced" with prescribed atmospheric data.

The initial conditions for the ocean are rest (no currents), with temperature and salinity from the Levitus (1982) January climatology. The sea ice is initialized with a realistic January 1 distribution of 95% (90%) concentration for the northern (southern) hemisphere, with a thickness of 2 m (1m), 0.2 m of snow cover, and an ice-surface temperature of -1 °C, and an interior ice snow energies consistent with temperatures of 0 °C. The atmospheric driving data are from the ERA-40 reanalysis (Uppala et al., 1999), interpolated to the geodesic grid. The model was integrated for four years with a 200-s time step for all components. We used a 250-km grid-spacing.

Figure 5 shows the mean January and July sea surface temperature maps from the NOAA data (1971 - 2000 mean), and the simulation (four-year mean). The tropical patterns are well reproduced, cold in the eastern part of the basins and warmer in the west, but the cold bias in the tropics is evident. Analysis shows that the simulated cooling is associated with an excessive deepening of the tropical mixed layer.

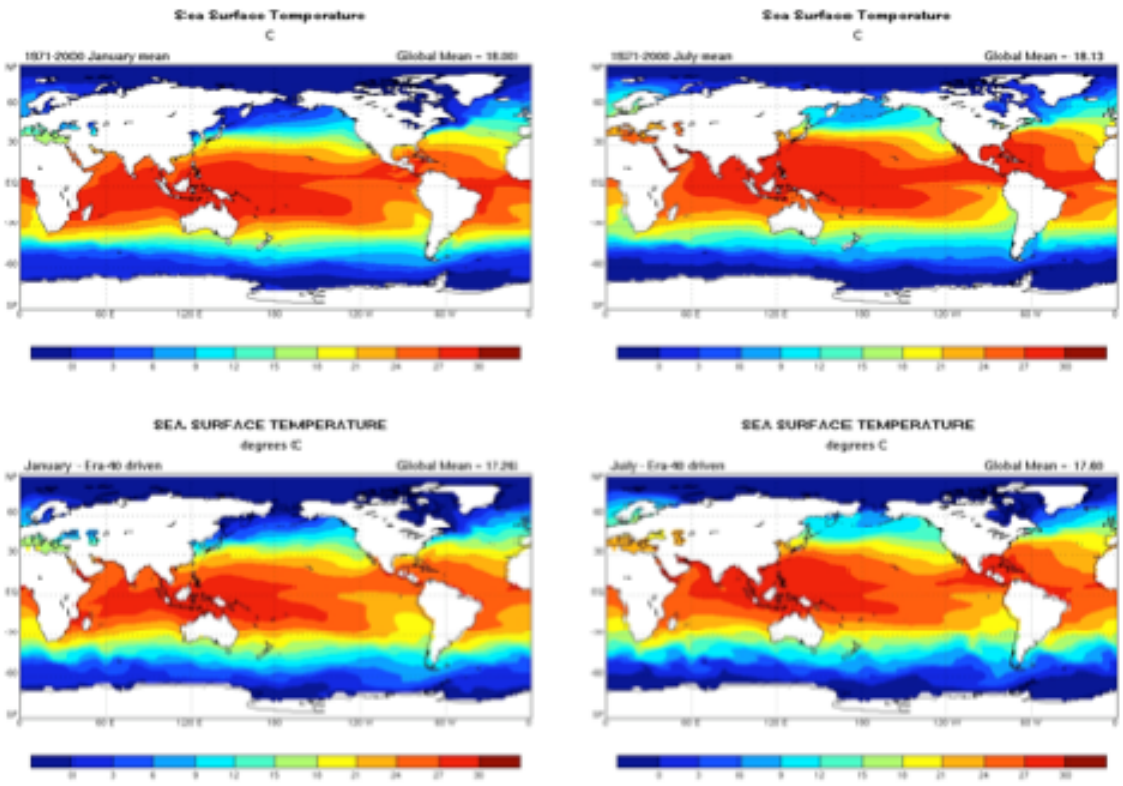

Figure 5: January (left column) and July (right column) sea surface temperature. At the top is the 1971-2000 mean from NOAA, in the middle is the 4-year mean from the data-driven ocean and sea ice models, and at the bottom the fully coupled model 2-year mean.

The tests described above set the stage for the coupled simulation described in the next section.

3.3 A One-Year Coupled Simulation

In our coupled simulation, the atmosphere was initialized using a January 1 restart record from an earlier long run in which the atmosphere model was driven using observed sea-surface temperatures, as described in Section 3.2 above. Similarly, the ocean model was initialized using a January 1 restart from an earlier run in which it had driven with ERA-40 re-analysis data (Upalla et al., 1999), as described in Section 3.2 above.

The simulated sea-surface temperature (SST) distribution is shown in Figure 6, along with the observations of Reynolds and Smith (1995). Figure 7 shows the difference between the first and second Januaries of the simulation. The pattern of the difference resembles an El Niño in the tropics, with warming west of South America, and a broad cooling over the remainder of the Pacific basin. This response is triggered by the "shock" of initialization, which excites a Kelvin wave in the Equatorial Pacific. The wind stress of the atmospheric model responds in a realistic fashion, as shown in Figure 8.

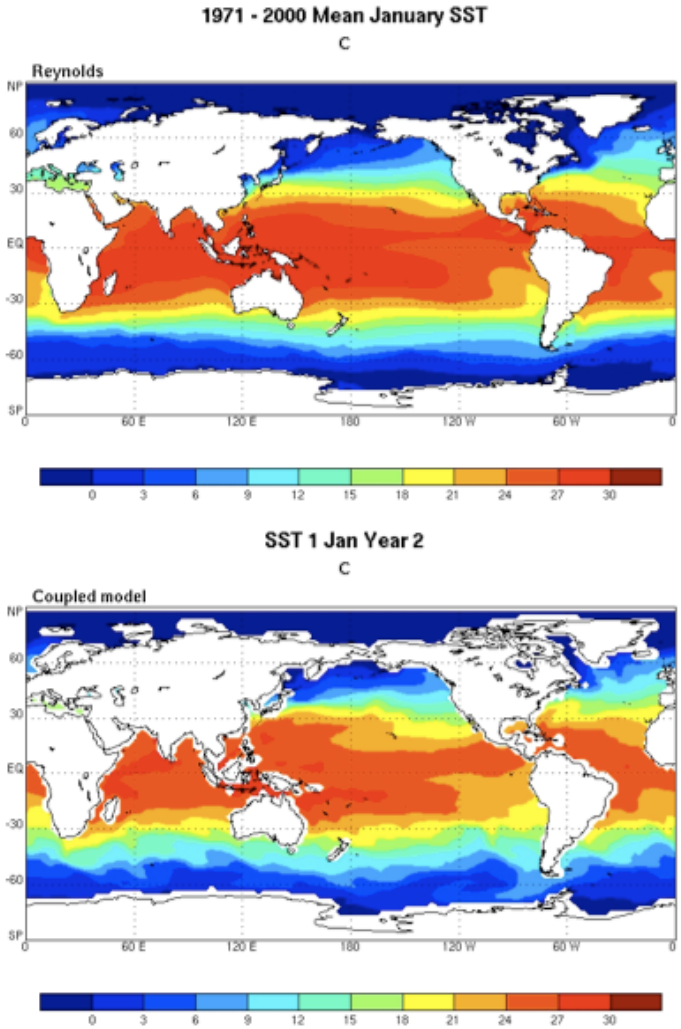

Figure 6: Simulated sea-surface temperature distribution. The top panel shows the January sea-surface temperature (SST) climatology for the period 1971-2000 according to Reynolds and Smith (1995). The bottom panel shows the SST distribution for 1 January of year 2 of the coupled model simulation.

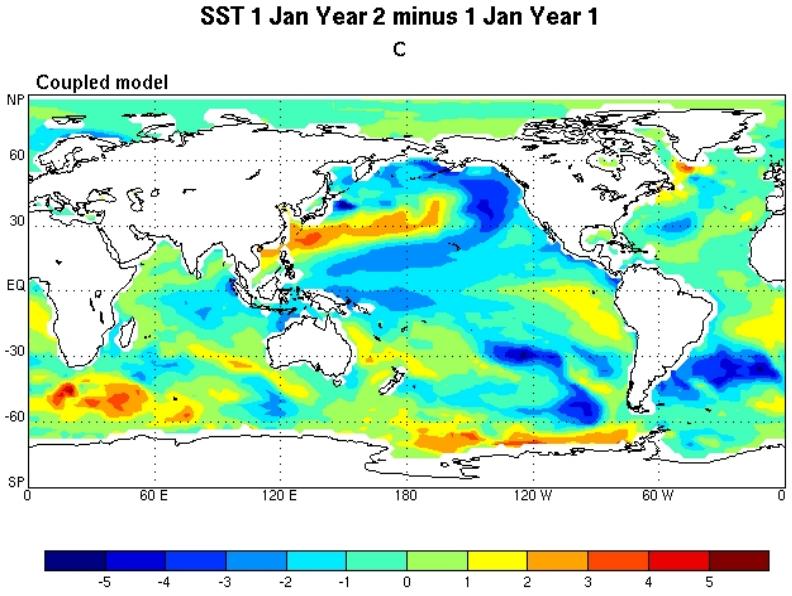

Figure 7: The SST difference between 1 January year 2 and 1 January year 1 of the coupled model simulation.

3.4 Discussion

We are now preparing a new, longer coupled simulation in which updated versions of both the atmosphere and ocean models are used. In preparation for this, we are also doing a much longer run in which the ocean model is driven with ERA-40 data.

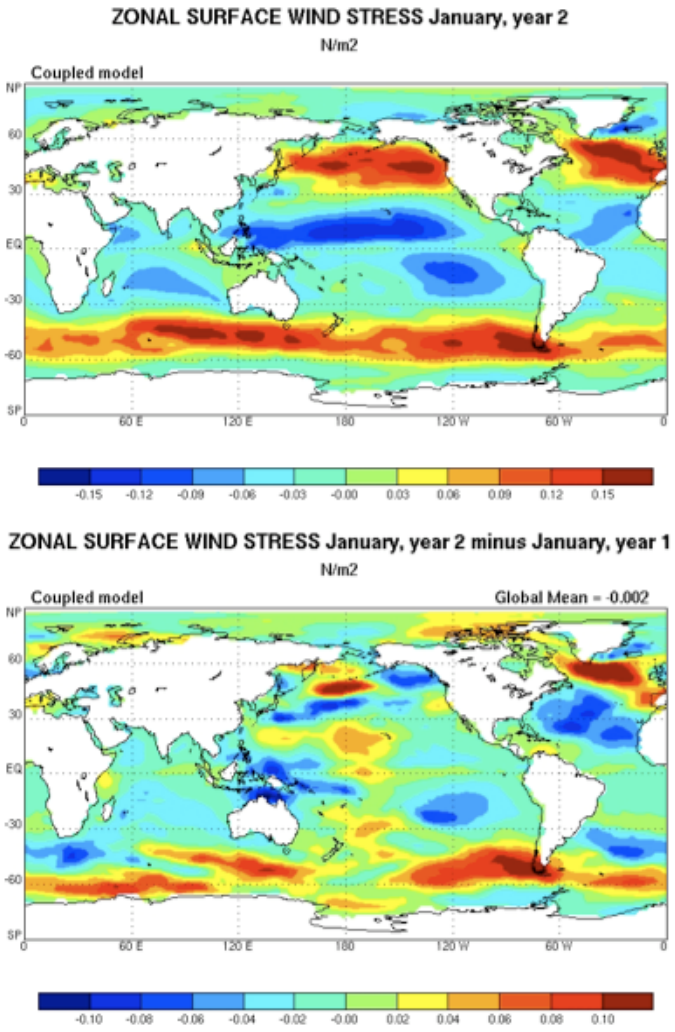

Figure 8: The wind stress of the atmospheric model. The upper panel shows the simulated zonal wind stress at the beginning of the second year of simulation, and the lower panel shows the difference relative to the beginning of the first year.

3.5 References

Ding, P, and DA Randall. 1998. "A cumulus parameterization with multiple cloud base levels." *J. Geophys. Res*. **103**, 11341-11354.

Fowler, LD, DA Randall, and SA Rutledge. 1996. "Liquid and ice cloud microphysics in the CSU general circulation model. part 1: model description and simulated microphysical processes." *J. Climate*. **9**, 489-529.

Gates, WL. 1992. "AMIP: The atmospheric model intercomparison project." *Bull. Amer. Meteor. Soc.*, **73**, 1962 - 1970.

Heikes, RP, and DA Randall. 1995. "Numerical integration of the shallow water equations on a twisted icosahedral grid. Part I: Basic design and results of tests." *Mon. Wea. Rev.* **123**, 1862-1880.

Hunke, EC, and JK Dukowicz. 1997. "An elastic-viscous-plastic model for sea ice dynamics." *J. Phys. Oceanogr.* **27**, 1849-1867.

Jones, PW. 1999. "First- and second-order conservative remapping schemes for grids in spherical coordinates." *Mon. Wea. Rev.* **127**, 2204-2210.

Large, WG, JC McWilliams, and SC Doney. 1994. "Oceanic vertical mixing: a review and a model with a nonlocal boundary layer parameterization." *Rev. Geophys.* **32**, 363-403.

Levitus, S. 1982. "Climatological atlas of the world oceans." *NOAA Prof. Paper 13,* U. S. Govt. Printing Office, Washington, D.C.

Palmer, TN, GJ Shutts, and R Swinbank. 1986. "Alleviation of a systematic westerly bias in general circulation and numerical weather prediction models through an orographic gravity wave drag parametrization." *Quart. J. R. Met. Soc.* **112**, 1001-1039.

Pan, D-M, and DA Randall. 1998. "A cumulus parameterization with a prognostic closure." *Quart. J. Roy. Met. Soc.* **124**, 949-981.

Randall, DA, TD Ringler, RP Heikes, P Jones, and J Baumgardner. 2002. "Climate modeling with spherical geodesic grids." *Computing in Science Engr.* **4**, 32-41.

Reynolds, RW, and TM Smith. 1995. "A high resolution global sea surface temperature climatology." *J. Climate.* **8**, 1571-1583.

Ringler, TD, RP Heikes, and DA Randall. 2000. "Modeling the atmospheric general circulation using a spherical geodesic grid: A new class of dynamical cores." *Mon. Wea. Rev.* **128**, 2471-2490.

Sellers, PJ, DA Randall, GJ Collatz, J Berry, C Field, DA Dazlich, C Zhang, and L Bounoua. 1996. "A revised land-surface parameterization (SiB2) for atmospheric GCMs. part 1: model formulation." *J. Climate.* **9**, 676-705.

Semtner, AJ Jr. 1976. "A Model for the thermodynamic growth of sea ice in numerical investigations of climate." *J. Phys. Oceanogr.* **6**, 379-389.

Stephens, GL, PM Gabriel, and PT Partain. 2001. "Parameterization of atmospheric radiative transfer. Part I: validity of simple models." *J. Atmos. Sci.* **58**, 3391 - 3409.

Uppala, S, JK Gibson, M Fiorino, A Hernandez, P Kållberg, X Li, K Onogi, and S Saarinen. 1999. "ECMWF second generation reanalysis—ERA40." *Proc. Second WCRP Int. Conf. on Reanalyses,* Wokefield Park, United Kingdom, WCRP. 9–13.

Appendix A: Model Description

The geodesic grid can be decomposed into logically rectangular subdomains, which are used to do memory allocation on a computer. Each subdomain can be decomposed in two dimensions. The model runs in a multiple-processor environment using the message passing interface (MPI).

The atmosphere sub-model includes prognostic equations for potential temperature, vorticity and divergence, surface pressure, specific humidity, cumulus kinetic energy (CKE), mixing ratios of cloud water, cloud ice, rain and snow, and the planetary boundary layer (PBL) depth. The discretization of the advection is highly conservative. The vertical coordinate is a generalized sigma coordinate, in which the PBL top is a coordinate surface. There are 29 layers, with the model top at 1 mb.

Deep moist convection is parameterized using a modified Arakawa-Schubert scheme with ice, prognostic CKE, cumulus friction, and multiple cloud bases (Pan and Randall, 1998; Ding and Randall, 1998). The large-scale cloud microphysical scheme is the one developed by Fowler et al. (1996), with cumulus detrainment as a source of cloud water and/or ice. The radiation is the Stephens (2001) parameterization. Gravity-wave drag is parameterized with a simple Palmer-like scheme (Palmer et al., 1986). Further details are given by Ringler et al. (2000) and Randall et al. (2002).

The ocean sub-model has prognostic equations for momentum, temperature, salinity and the free surface height. Depth is used as the vertical coordinate, with 33 layers. Horizontal transport is done by monotone flux-corrected transport and vertical transport by monotone remapping. KPP (Large et al., 1994) is used to parameterize the ocean boundary-layer turbulence and convection.

The sea ice sub-model predicts ice concentration, volume and energy content. There are four ice layers, and snow is accumulated on the ice. The dynamics are based on the elastic-viscous-plastic rheology (Hunke and Dukowicz, 1997). The thermodynamics are based on Semtner (1976). Flux-corrected transport is used to advect the ice.

In addition, CCoSM includes a sub-model for land-surface processes, SiB2, which was developed by Sellers et al. (1996). SiB2 includes parameterizations of canopy physiological responses (photosynthesis, stomatal conductance), and was designed to utilize satellite measurements for many of the important vegetation boundary conditions such as fraction of short wave radiation absorbed, leaf area index, albedo and roughness.

The integrations of these several components are coordinated by a software component called a coupler. On every time step, variables needed to compute the fluxes of mass, momentum and energy between components are passed to the coupler. The coupler computes these fluxes and sends them to the components. To deal with possible differences in resolution, a conservative interpolation is performed using SCRIP, which was developed at the Los Alamos National Laboratory (Jones, 1999). The PBL parameterization, which determines the surface fluxes, PBL-top entrainment rate, and PBL-cloudiness, is implemented in the coupler.

The coupler can also be used to replace climate components with prescribed data. For instance, the dynamic ocean and sea ice modules can be replaced with prescribed sea surface temperature and ice cover

to drive the atmosphere; the dynamic atmosphere can be replaced with prescribed surface air conditions, radiative fluxes and precipitation to drive the ocean. In the tests described below, the coupler was used in this way.